Turbulence and bias-induced flows in simple magnetized toroidal plasmas

B. Li, B. N. Rogers, P. Ricci, K. W. Gentle, and A. Bhattacharjee

Turbulence and bias-induced flows in simple magnetized toroidal plasmas

B. Li,[1] B. N. Rogers,[1] P. Ricci,[2] K. W. Gentle,[3] and A. Bhattacharjee[4]

[1] *Department of Physics and Astronomy, Dartmouth College, Hanover, New Hampshire 03755, USA*
[2] *Centre de Recherches en Physique des Plasmas - École Polytechnique Fédérale de Lausanne,*
Association EURATOM-Confédération Suisse, CH-1015 Lausanne, Switzerland
[3] *Department of Physics, Institute for Fusion Studies,*
University of Texas at Austin, Austin, Texas 78712, USA
[4] *Department of Physics, University of New Hampshire, Durham, New Hampshire 03824, USA*

Turbulence and bias-induced flows in simple magnetized toroidal plasmas are explored with global three-dimensional fluid simulations, focusing on the parameters of the Helimak experiment. The simulations show that plasma turbulence and transport in the regime of interest are dominated by the ideal interchange instability. Application of a bias voltage alters the structure of the plasma potential, resulting in the equilibrium sheared flows. These bias-induced vertical flows appear to reduce the radial extent of density and temperature fluctuations, and thereby lower the particle and heat transport.
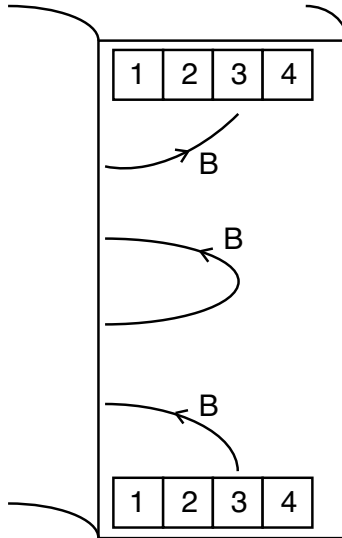
FIG. 1. Schematic cross section of the Helimak showing the geometry and a helical field line. The plates labeled 1-4 are isolated from each other and can be independently biased.

I. INTRODUCTION

Turbulence suppression by sheared flows is of considerable interest in plasma physics and in fluid dynamics in general, affecting such diverse fields as planetary atmospheres and fusion plasma confinement [1, 2]. The shear magnitude (the gradient) of the flow is often expected to increase in order to suppress plasma turbulence. However, recent Helimak experiments observe that turbulence reductions can be driven by negative biasing and the bias-induced equilibrium flows with shear magnitudes comparable to the unbiased case are sufficient to reduce plasma fluctuations [3]. This unexpected observation is possibly because the nature of the interchange instability in the Helimak device is radially global, and the mean $\boldsymbol{E} \times \boldsymbol{B}$ flows are generated by an equilibrium electric potential arising from the sheath boundary conditions [4, 5]. In this paper, we simulate the impact of an externally imposed bias voltage on the interchange-driven turbulence and transport in the Helimak device. The global nonlinear fluid simulations presented here show similar bias-induced transitions to the states of reduced turbulence and transport, consistent with Helimak observations.

Simple magnetized torus (SMT) experiments [6–8] such as the Helimak [3, 9, 10] provide opportunities to study the basic physics of plasma turbulence and transport in a simplified magnetic configuration that is most similar to the scape-off layer (SOL) of tokamaks. In the SMT configuration, a small vertical field B_v is added to a dominant toroidal field B_φ. The helical, open field lines wind around the symmetry axis and terminate on the top and bottom of the vessel. The pitch of the field line is given by $\Delta = 2\pi R B_v / B_\varphi = L_v / N$ where R is the vessel major radius, L_v is the vessel height, and N is the total number of toroidal turns made by a field line from bottom to top. Figure 1 shows the Helimak geometry: the toroidal chamber has a rectangular cross section spanning the major radius R from 0.6 to 1.6 m and a height L_v of 2 m. The field strength generated by external currents decreases with the radius as $B \propto 1/R$. Four sets of four conducting plates are installed radially at the top and bottom vessel walls. The plates support a large number of Langmuir probes for measuring plasma properties. In this device the plasma potential on the (open) field lines can be affected by biasing the plates on which the field lines terminate. For normal grounded operation, all the plates are connected to the vessel ground. An equilibrium electric potential $\phi \propto T_e$ results from the sheath boundary conditions [11], resulting in vertical, sheared $\boldsymbol{E} \times \boldsymbol{B}$ flows. For biased operation, the plates within a chosen range of R are connected to a bias voltage. This bias induces a radial electric field that can strongly impact the potential profile and the vertical $\boldsymbol{E} \times \boldsymbol{B}$ flows. The time traces of plasma density show that the fluctuations are reduced when the bias voltage, and thus the sheared $\boldsymbol{E} \times \boldsymbol{B}$ flows, are made sufficiently large. The turbulence reduction is a bifurcation. It is complete by the bias voltage ~ -20 V; the fluctuation levels for the -20 V and the larger bias voltage are indistinguishable. The experimental results from biasing are described in detail in Refs. [3, 9].

The magnetic curvature and pressure gradient on the low field (large R) side of the chamber give rise to the

interchange instability with $k_\parallel \simeq 0$ and typical growth rates $\gamma \sim c_s/\sqrt{RL_p}$ where $c_s = \sqrt{T_e/m_i}$ is the sound speed and L_p is the pressure scale length. In the unbiased case, the interchange instability in the SMT was initially simulated with electrostatic two-dimensional (2D) fluid model [5, 12, 13] that includes plasma sources and parallel losses. Similar fluid models are also used to study the interchange instability in the SOL of tokamaks [14, 15]. In the 2D simulations of the SMT configuration, the vertical extent of the simulation domain is controlled by the pitch of the fieldlines: assuming $k_\parallel = 0$, all quantities must be periodic in the vertical direction on the length scale L_v/N. In the experiment, however, the periodicity is eventually broken by the upper and lower walls. This has motivated more recent, non-periodic global three-dimensional (3D) fluid simulations, in which the vertical simulation domain is the full height of the chamber [4]. These simulations, like those presented here, show that the transport driven by interchange modes is strong enough to prevent the pressure gradients from ever steepening into the drift-wave regime [4].

The simulations of plasma dynamics in the Helimak device, as in Ref. [4], evolve the various quantities with no separation made between perturbations and equilibrium, and can thus explore the self-consistent evolution of the plasma and potential profiles in the presence of the plasma sources, the transport produced by plasma instabilities, the (sonic) plasma losses at the sheaths, and the externally applied bias voltage. In the unbiased case, the simulations show that the turbulent structures of the density and temperature driven by the interchange mode are bursty, and have relatively wide radial extents on the low field (large R) side. In the case with negative biasing, both the simulations and experiment show that the bias-induced equilibrium flows with velocity shear magnitudes comparable to the unbiased case are sufficient to reduce the interchange-driven turbulence and transport. Although the magnitudes of velocity shear appear to be not that different globally, the snapshots of global simulations reveal that the plasma potential structures are completely different in the two cases: the streamlines of the $\boldsymbol{E} \times \boldsymbol{B}$ velocities are mostly closed in the unbiased case, while in the biased case the streamlines are completely open at the top and bottom boundaries, indicating enhanced plasma losses at the bias plates caused by the vertical flows. The simulations restarted from the biased case show that once the bias voltage is removed from the boundary condition, the plasma potential structures quickly return to the normal unbiased state and consequently strong convective transport of the plasma resumes on the low field side. This indicates that in the biased case the pressure profiles are still strongly unstable to interchange instabilities. However, the application of the external bias alters the structures of the plasma potential, resulting in the equilibrium sheared flows. These bias-induced vertical flows located in the gradient region (the edge region of plasma sources) appear to reduce the radial extent of turbulent zone, and thereby also reduce the transport of the density and temperature across the magnetic field.

This paper is organized as follows. In Sec. II, we review the electrostatic fluid model used in the simulations. In Sec. III we describe the nonlinear simulations of the Helimak experiment for the grounded and biased cases. The final section summarizes our findings.

II.   MODEL EQUATIONS

For singly ionized argon, typical Helimak plasma parameters are $n \sim 10^{10}$ cm^{-3}, $T_i \sim 0.1$ eV, $T_e \sim 10$ eV, and $\beta \sim 10^{-5}$. The small β and T_i values in the experiment lead us to consider the drift-reduced Braginskii equations [16, 17] with cold ions $T_i = 0$ and an electrostatic electric field $\boldsymbol{E} = -\nabla\phi$. The resulting fluid model consists of the electron continuity equation

$$\frac{dn}{dt} + \nabla \cdot (n\boldsymbol{v}_{de}) + n\nabla \cdot \boldsymbol{v}_E + \nabla_\parallel(nv_{\parallel e}) = 0 \, , \tag{1}$$

the vorticity equation

$$\nabla \cdot (\boldsymbol{j}_p + \boldsymbol{j}_d) + \nabla_\parallel j_\parallel = 0 \, , \tag{2}$$

the electron temperature equation

$$\frac{3}{2}n\frac{d^e T_e}{dt} = T_e\frac{d^e n}{dt} + \frac{5}{2}\frac{p_e}{e}\hat{C}T_e + \frac{0.71}{e}T_e\nabla_\parallel j_\parallel \, , \tag{3}$$

the parallel component of electron momentum equation, i.e., Ohm's law

$$\frac{ej_\parallel}{\sigma_\parallel} = -e\nabla_\parallel\phi + \frac{\nabla_\parallel p_e}{n} + 0.71\nabla_\parallel T_e + m_e\frac{d^e}{dt}v_{\parallel e} \, , \tag{4}$$

and the parallel ion momentum equation

$$m_i n\frac{d^i}{dt}v_{\parallel i} = -\nabla_\parallel p_e \, , \tag{5}$$

where

$$\frac{d^e}{dt} = \frac{d}{dt} + v_{\|e}\nabla_\| \;, \qquad \frac{d^i}{dt} = \frac{d}{dt} + v_{\|i}\nabla_\| \;,$$

$$\frac{d}{dt} = \frac{\partial}{\partial t} + \boldsymbol{v}_E \cdot \nabla \;, \qquad \hat{C} = \left(\nabla \times \frac{c\boldsymbol{b}}{B}\right)\cdot \nabla \;,$$

$\boldsymbol{v}_E = (c/B)\boldsymbol{E}\times\boldsymbol{b}$ is the $\boldsymbol{E}\times\boldsymbol{B}$ velocity, $p_e = nT_e$ is the electron pressure, $\boldsymbol{j}_d = -en\boldsymbol{v}_{de} = (c/B)\boldsymbol{b}\times\nabla p_e$ is the diamagnetic current with $T_i = 0$, $\boldsymbol{v}_{de}$ is the electron diamagnetic drift, $j_\| = en(v_{\|i} - v_{\|e})$ is the parallel current, $\sigma_\|$ is the parallel conductivity, $\boldsymbol{j}_p = en\boldsymbol{v}_p$ is the polarization current, $\boldsymbol{v}_p = (c/B\Omega_i)d^i\boldsymbol{E}_\perp/dt$ is the ion polarization drift with $T_i = 0$. In the presence of magnetic-field gradient and curvature, $\nabla\cdot\boldsymbol{v}_E = \hat{C}\phi$ and $\nabla\cdot\boldsymbol{j}_d = \hat{C}p_e$. For $\nabla\times\boldsymbol{B} = 0$ with negligible local current $\nabla\times(\boldsymbol{b}/B) = 2(\boldsymbol{b}\times\boldsymbol{\kappa})/B$ where $\boldsymbol{\kappa} = (\boldsymbol{b}\cdot\nabla)\boldsymbol{b}$ is the fieldline curvature. Here the divergence of the polarization current is approximated as $\nabla\cdot\boldsymbol{j}_p \approx (-enc/B\Omega_i)d^i\nabla_\perp^2\phi/dt$ [5]. At the ends of the open field lines, Bohm sheath boundary conditions are applied to the parallel ion and electron velocities [11, 18] $v_{\|i} = \pm c_s$ and $v_{\|e} = \pm c_s\exp[\Lambda + e(V_b - \phi)/T_e]$ where $\Lambda = \log\sqrt{m_i/2\pi m_e} \simeq 3$ and V_b is the bias voltage. The plus and minus signs indicate that parallel velocities are in opposite directions at the top and bottom walls.

In the simulations, T_e and $e\phi$ are normalized to a fixed reference value T_{e0}, the density n to n_0, the time to R/c_s, the parallel length to R, the parallel speed to c_s, the perpendicular length to $\rho_s = c_s/\Omega_i$ where $c_s = \sqrt{T_{e0}/m_i}$ and $\Omega_i = eB/m_ic$. The simulations use field-aligned coordinates in which $\hat{z}$ is the parallel direction along the field line, $\hat{x}$ is the radial direction of major radius, and $\hat{y}$ is perpendicular to both $\hat{x}$ and $\hat{z}$ (for strong toroidal fields $\hat{y}$ is approximately the vertical direction). For consistency with the experiment the magnetic field direction is taken as $\boldsymbol{b} = -\hat{z}$ and thus the the curvature operator is $\hat{C} = 2\partial/\partial y$ [5]. Spatially localized source terms S_n and S_T are added to the density and temperature equations to model the particle and heat sources in the experiments. The final dimensionless equations for the full plasma density, electric potential, electron temperature, and parallel velocities are [4, 19]

$$\frac{dn}{dt} = \hat{C}p_e - n\hat{C}\phi - \nabla_\|(nv_{\|e}) + S_n \;, \tag{6}$$

$$\frac{d^i}{dt}\nabla_\perp^2\phi = \frac{\hat{C}p_e}{n} + \frac{\nabla_\| J}{n} \;, \tag{7}$$

$$\frac{d^e}{dt}T_e = \frac{2}{3}T_e\left(\frac{\hat{C}p_e}{n} - \hat{C}\phi - \nabla_\| v_{\|e}\right)$$
$$+ \frac{2}{3}T_e\left(\frac{5}{2}\hat{C}T_e + 0.71\frac{\nabla_\| J}{n}\right) + S_T \;, \tag{8}$$

$$\frac{m_e}{m_i}\frac{d^e}{dt}v_{\|e} = \nu J + \nabla_\|\phi - \frac{\nabla_\| p_e}{n} - 0.71\nabla_\| T_e \;, \tag{9}$$

$$\frac{d^i}{dt}v_{\|i} = \frac{-\nabla_\| p_e}{n} \;, \tag{10}$$

where $d/dt = \partial/\partial t + (R/\rho_s)\boldsymbol{v}_E\cdot\nabla_\perp$, the $\boldsymbol{E}\times\boldsymbol{B}$ velocity $\boldsymbol{v}_E = \nabla\phi\times\hat{z}$, $J = n(v_{\|i} - v_{\|e})$, $\nu = e^2n_0R/(c_sm_i\sigma_\|)$, $\nabla_\| = \partial/\partial z$ and $\nabla_\perp = \hat{x}\partial/\partial x + \hat{y}\partial/\partial y$. The source profiles S_n and S_T are assumed to have the Gaussian form: $S_0\exp[-(x - x_s)^2/x_0^2]$ where S_0 is the source production rate. The bias profile takes the form of a step function: $V_b\{\tanh[(x - x_{\min})/x_b] + \tanh[(x_{\max} - x)/x_b]\}/2$. The global simulation domain encompasses the full radial, vertical, and toroidal extent of the device. At $x = 0$ and $x = L_x$, Neumann boundary conditions are imposed for the parallel velocities and Dirichlet boundary conditions for the other quantities. At $y = 0$ and $y = L_y$, for the parallel velocities we use Bohm boundary conditions $v_{\|i} = \pm\sqrt{T_e}$ and $v_{\|e} = \pm\sqrt{T_e}\exp[\Lambda + (V_b - \phi)/T_e]$; for the plasma potential we impose $\phi = \Lambda T_e + V_b$ (implying $v_{\|e} = v_{\|i}$). In the simulations, small perpendicular diffusion terms are added to the evolution equations for each quantity, and a constant nominal pitch is used across the radius. For the biased case, we vary only the strength of the bias voltage in the simulation, represented by the parameter V_b. In both the
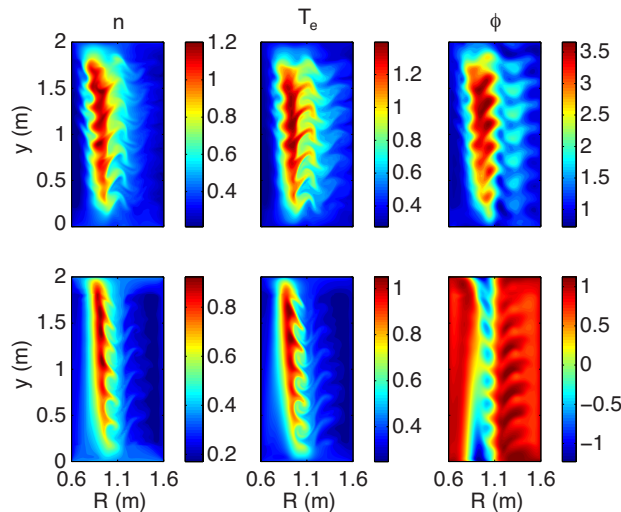
FIG. 2. (Color online) Typical snapshots of density n (left), electron temperature T_e (center), and plasma potential ϕ (right) in the cross section for zero bias (upper panels) and bias $V_b = -3$ (lower panels).

grounded and biased cases, extra diffusion layers are added at the top and bottom edges to remove the accumulation of plasma at the vertical boundaries due to the vertical flows. This may cause the observed smaller values of density and temperature in the simulations with bias. Assuming $k_\parallel = 0$ the 3D model equations reduce to the electrostatic 2D models noted earlier [5, 12]. The code used here has already been applied to the simulation of the TORPEX SMT configuration [4, 19]. Equations (6)-(10) are solved using a finite difference scheme. The $\boldsymbol{E} \times \boldsymbol{B}$ convective term is treated using the Arakawa advection scheme, while the parallel convective terms are discretized with a second order centered difference method. Time is advanced using a standard explicit Runge-Kutta stepping.

For typical Helimak argon discharges, $T_{e0} \simeq 10$ eV, $\rho_s \simeq 2$ cm, $c_s \simeq 4.9 \times 10^3$ m/s, $R/c_s \simeq 0.2$ ms, the electron collisional time $\tau_e \sim 0.01$ ms, which gives the dimensionless resistivity parameter $\nu \sim 10^{-4}$. The parameters used in the simulations are $R = 55\rho_s$, $L_x = 50\rho_s$, and $L_y = 2L_x$. The number of field line turns $N = 8$ corresponds to a nominal pitch of about $12\rho_s \simeq 0.2$ m. For the source profiles, we set $S_n = S_T$ with the source strength $S_0 = 0.1$, the maximum location $x_s = 0.9$ m, and the width $x_0 = 0.1$ m. Following the experiment, the bias is applied near the source locations from $x_{\min} = 0.86$ m to $x_{\max} = 1.06$ m with the edge width $x_b = 0.1$ m. The mass ratio m_e/m_i arises in the parallel electron momentum equation (9) due to the normalization. The nominal small values $m_e/m_i = 1/200$ and $\nu = 0.01$ are used to ensure numerical convergence. The simulation results are independent of m_e/m_i and ν because the simulations are dominated by ideal interchange dynamics, which is not affected by these parameters.

III. NONLINEAR SIMULATION

The simulations are normally started from small random perturbations with initial profiles that are uniform in the y direction. The pressure profiles steepen due to the sources until the interchange instabilities are triggered. These instabilities produce intermittent convective transport of plasma from the source region to the low field side, and the plasma is eventually removed from the system by the parallel flows to the ends of the open field lines. After a transient period, a nonlinearly saturated stationary state is reached in which the fluctuations have broad frequency spectra [20, 21] and non-Gaussian probability distributions [5]. The simulation results described here focus on the statistically steady state.

Figure 2 shows typical snapshots of density n, electron temperature T_e, plasma potential ϕ in the cross section of the device. Away from the walls of the plasma chamber, the spatial structures at these parameters are approximately periodic over a vertical distance L_v/N and have toroidal wavelengths $2\pi R$, consistent with the $k_\parallel \simeq 0$ nature of the interchange modes noted earlier [4]. The evolution of turbulence driven by the interchange instability displays an intermittent (bursty) character [14]. During the burst shown in Fig. 2, the particles and heat are lost by convective transport from the source region to the low field side. This produces large fluctuations and strong profile relaxation. Such bursts of density and temperature transport are followed by a relatively quiet period during which the unstable density and temperature structures rebuild. The process then repeats. In the grounded case, the contours of the plasma potential exhibit large-scale velocity eddies or convection cells. The streamlines of the $\boldsymbol{E} \times \boldsymbol{B}$ velocity are
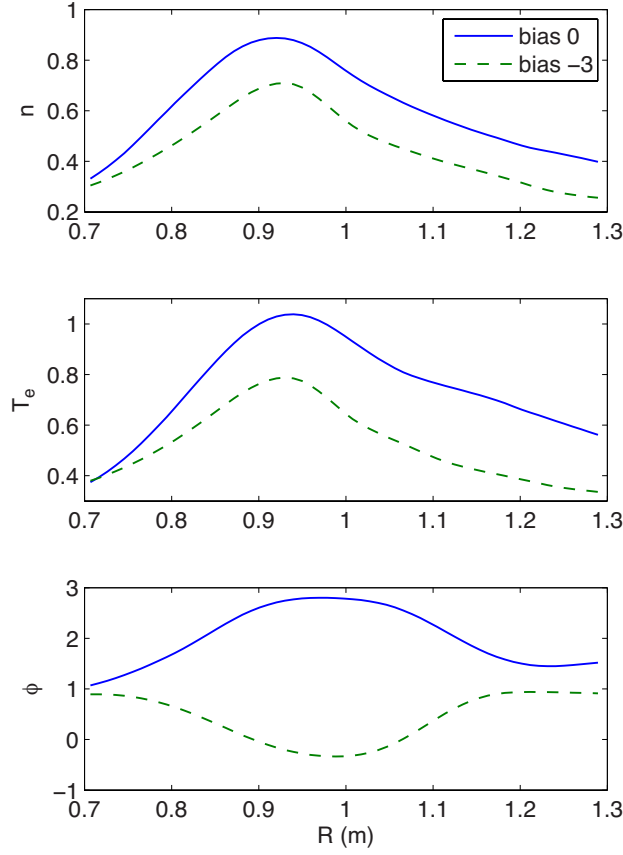
FIG. 3. (Color online) Typical profiles of density n, electron temperature T_e, and plasma potential ϕ for zero bias (solid line) and bias $V_b = -3$ (dashed line).

nearly closed loops. The coherent turbulent structures of density and temperature have relatively wide radial extents on the low field side. In the biased case, the closed potential contours progressively open up at the upper and lower bias locations, since the bias voltage induces equilibrium radial electric fields between the biased region and the adjacent plasma. When the bias voltage is made sufficiently large (here $V_b = -3$), the biased state is reached in which the bias-induced vertical $\boldsymbol{E} \times \boldsymbol{B}$ flows pass through the plasma interior from the top and bottom boundaries. These equilibrium sheared flows appear to reduce the radial extent of turbulent structures; that is, the bias tends to reduce the radial correlations and increase the vertical correlations, as observed in the experiment [3]. Following the experiment, the transitions of plasma dynamics between the biased and grounded states are also simulated. The simulations restarted from the biased state show that once the bias is turned off the structures of potential and pressure quickly return to the original grounded state.

Figure 3 shows typical time-averaged profiles of density $\langle n \rangle$, electron temperature $\langle T_e \rangle$, and plasma potential $\langle \phi \rangle$. Here $\langle \cdots \rangle$ indicates the averages over time and the vertical direction. The density and temperature peaks follow the source maximum, and the radial convective transport broadens the density and temperature profiles. In the unbiased case, the potential maximum follows the electron temperature $\phi \sim \Lambda T_e$ due to Ohm's law and the sheath boundary conditions. In the biased case, the plasma potential moves in the direction of biasing with $\phi \sim \Lambda T_e + V_b$. The negative bias produces a potential minimum in the biased region.

Figure 4 shows typical density and electron temperature profiles in the experiment. The plasma potential cannot be directly measured in the experiment. Alternatively, as shown later one can compare the $\boldsymbol{E} \times \boldsymbol{B}$ flows resulting from the potential. In the Helimak, parallel flows to the top and bottom constitute a strong loss channel that is independent of radial turbulent transport. Thus the density and temperature profiles show only modest changes with transport reductions induced by biasing. The pressure profiles change slightly and the gradients of experimental profiles are larger with bias. That is, the drive for the interchange instability is not reduced in the biased case. The breadth of the plasma profiles in the Helimak experiment involves some complex physics including the electron-cyclotron and upper-hybrid resonances [9]. The source mechanisms and boundary conditions in the simulations are much simpler
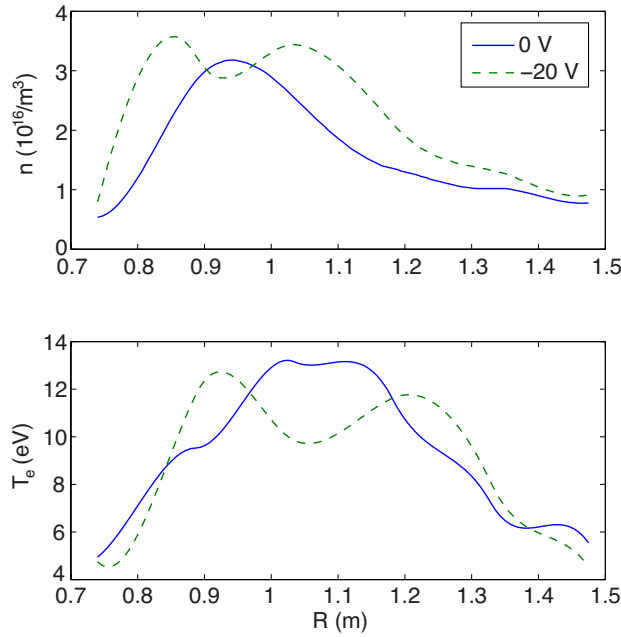
FIG. 4. (Color online) Typical experimental profiles of density n and electron temperature T_e for zero bias (solid line) and bias voltage -20 V (dashed line).

than those in the experiments. For this reason, our results should be regarded as only the first step toward modeling the biasing experiments.

The potential fluctuations generate the fluctuations in the vertical electric field and the radial $\boldsymbol{E} \times \boldsymbol{B}$ velocity $v_x = \partial \phi / \partial y$. This leads to turbulent convective transport of plasma across the magnetic field. Figure 5 shows typical time-averaged profiles of the radial particle flux $\Gamma_n = \langle n v_x \rangle$ in units of $n_0 c_s$ and heat flux $\Gamma_T = \langle T_e v_x \rangle$ in units of $T_{e0} c_s$. In the grounded state, the outward (positive) particle and heat fluxes increase sharply in the source region and reach a maximum on the low field side. In the biased state, the radial convective transport of the density and temperature is clearly reduced on the low field side.

Figure 6 shows typical time-averaged profiles of vertical $\boldsymbol{E} \times \boldsymbol{B}$ flow $v_E = -d\langle \phi \rangle / dx$ in units of c_s and velocity shear $v_E' = dv_E / dx$ in units of Ω_i. In the grounded case, the vertical flows reverse directions from upward on the low field side to downward on the high field side and thus produce a dominant positive velocity shear. The radial distance between the minimum and maximum of the flow indicates the radial extent of turbulent eddies (here about 0.25 m). In the biased case, the bias-induced radial electric fields change directions across the biased region and thus generate vertical, sheared $\boldsymbol{E} \times \boldsymbol{B}$ flows. The radial distance between the maximum and minimum of the bias-induced flow reflects the width of the biased region (here about 0.2 m). The negative bias produces a negative velocity shear at the bias location.

Figure 7 shows typical experimental profiles of vertical plasma flow and velocity shear. The mean flow is measured from the Doppler shift of the argon ion lines and the velocity measurement is vertically and time averaged. The observed profiles are quite similar to the simulations. In the biasing experiment, the plates second from the inside were connected together and biased over the radius R from 0.86 to 1.06 m. Applying a negative bias voltage ~ -20 V leads to the transition to a state in which plasma fluctuations decrease to a much lower level [3]. The global 3D simulations exhibit similar transitions: the negative bias $V_b = -3$ (corresponding to a physical voltage ~ -20 V in the Helimak) leads to the biased state in which radial convective transport is reduced.

IV. CONCLUSIONS

We have simulated the impact of an externally imposed bias voltage on the interchange-driven turbulence and transport in the Helimak device. The global 3D fluid simulations show that plasma turbulence and transport in the regime of interest are dominated by the ideal interchange instability. In the grounded case, the turbulent structures of the density and temperature driven by the interchange mode are bursty, and have relatively wide radial extents on the
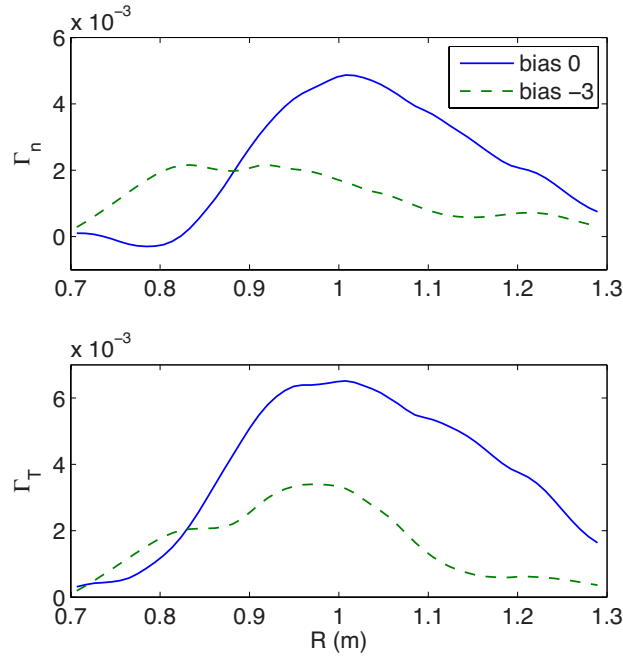
FIG. 5. (Color online) Typical profiles of radial particle flux Γ_n and heat flux Γ_T for zero bias (solid line) and bias $V_b = -3$ (dashed line).
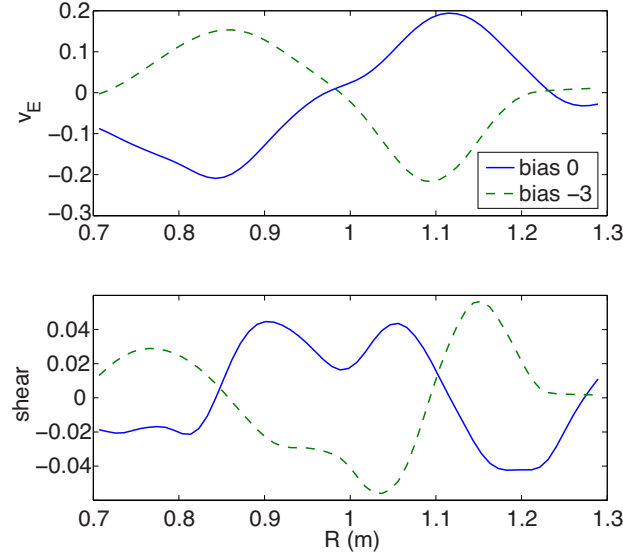

FIG. 6. (Color online) Typical profiles of vertical $\boldsymbol{E} \times \boldsymbol{B}$ flow v_E and velocity shear for zero bias (solid line) and bias $V_b = -3$ (dashed line).

low field side. In the biased case, a bias voltage is applied to the upper and lower boundaries over a small range of R. The structures of plasma potential are changed in response to the bias voltage, resulting in the equilibrium sheared flows. These bias-induced vertical flows appear to reduce the radial extent of turbulent structures, and thereby lower convective transport of particles and heat across the magnetic field, consistent with Helimak observations.
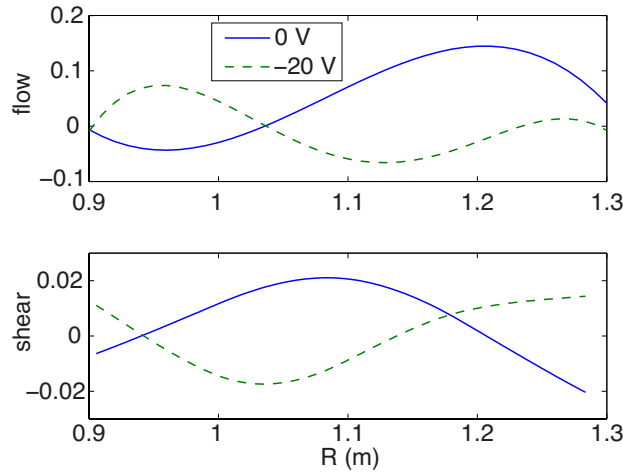
FIG. 7. (Color online) Typical experimental profiles of vertical flow and velocity shear for zero bias (solid line) and bias voltage -20 V (dashed line). The flow is normalized to $c_s \simeq 4.9 \times 10^3$ m/s and shear to $\Omega_i \simeq 2.4 \times 10^5$ s^{-1}.

ACKNOWLEDGMENTS

[1] P. W. Terry, Rev. Mod. Phys. **72**, 109 (2000).
[2] P. H. Diamond, S.-I. Itoh, K. Itoh, and T. S. Hahm, Plasma Phys. Control. Fusion **47**, R35 (2005).
[3] K. W. Gentle, K. Liao, K. Lee, and W. L. Rowan, Plasma Science and Technology **12**, 391 (2010).
[4] P. Ricci and B. N. Rogers, Phys. Rev. Lett. **104**, 145001 (2010).
[5] B. Li, B. N. Rogers, P. Ricci, and K. W. Gentle, Phys. Plasmas **16**, 082510 (2009).
[6] S. H. Müller, A. Fasoli, B. Labit, M. McGrath, M. Podestà, and F. Poli, Phys. Rev. Lett. **93**, 165003 (2004).
[7] K. Rypdal and S. Ratynskaia, Phys. Rev. Lett. **94**, 225002 (2005).
[8] F. M. Poli, P. Ricci, A. Fasoli, and M. Podestà, Phys. Plasmas **15**, 032104 (2008).
[9] K. W. Gentle and H. Huang, Plasma Science and Technology **10**, 284 (2008).
[10] J. C. Perez, W. Horton, K. W. Gentle, W. L. Rowan, K. Lee, and R. B. Dahlburg, Phys. Plasmas **13**, 32101 (2006).
[11] P. C. Stangeby, *The plasma boundary of magnetic fusion devices* (Institute of Physics, Berkshire, 2000).
[12] P. Ricci, B. N. Rogers, and S. Brunner, Phys. Rev. Lett. **100**, 225002 (2008).
[13] P. Ricci and B. N. Rogers, Phys. Plasmas **16**, 062303 (2009).
[14] O. E. Garcia, V. Naulin, A. H. Nielsen, and J. Juul Rasmussen, Phys. Rev. Lett. **92**, 165003 (2004).
[15] D. A. Russell, J. R. Myra, and D. A. D'Ippolito, Phys. Plasmas **16**, 122304 (2009).
[16] A. Zeiler, J. F. Drake, and B. Rogers, Phys. Plasmas **4**, 2134 (1997).
[17] A. Zeiler, *Tokamak Edge Turbulence* (IPP-Report 5/88, Max-Planck-Institut für Plasmaphysik, 1999).
[18] M. A. Lieberman and A. J. Lichtenberg, *Principles of Plasma Discharges and Materials Processing* (Wiley, New York, 1994).
[19] P. Ricci and B. N. Rogers, Phys. Plasmas **16**, 092307 (2009).
[20] B. Li and R. D. Hazeltine, Phys. Rev. E **73**, 065402 (2006).
[21] B. Li, R. D. Hazeltine, and K. W. Gentle, Phys. Rev. E **76**, 066402 (2007).